Tuning Gold Nanoparticle–Poly(2-hydroxyethyl methacrylate) Brush Interactions: From Reversible Swelling to Capture and Release

Steve Diamanti,[†] Shafi Arifuzzaman,[‡] Jan Genzer,[‡] and Richard A. Vaia[†,*]

[†]Air Force Research Laboratory, Materials and Manufacturing Directorate, 2941 Hobson Way, Wright-Patterson Air Force Base, Ohio, and [‡]Department of Chemical and Biomolecular Engineering, North Carolina State University, 911 Partners Way, Raleigh, North Carolina

ABSTRACT Tailoring the interaction between surfaces and nanoparticles (NPs) affords great opportunities for a range of applications, including sensors, information storage, medical diagnostics, and filtration membranes. In addition to controlling local ordering and microscale patterning of the NPs, manipulating the temporal factors determining the strength of the interaction between NP and surface enables dynamic modulation of these structural characteristics. In this contribution we demonstrate robust polymer brush-NP hybrids that exhibit both reversible swelling and reversible NP adsorption/desorption. Polymer brush functionality is tailored through post-functionalization of poly(2-hydroxyethyl methacrylate) (PHEMA) brushes on flat solid substrates with alpha-amine conjugates ranging from perfluoro alkanes to poly(ethylene glycol) of varying molecular weights. The type of functionality controls NP affinity for the surfaces. In the case of poly(ethylene glycol) (PEG), the molecular weight (MW) of the PEG dictates adsorption and desorption phenomena. Higher MW PEG chains possess increased binding affinity toward NPs, which leads to higher relative Au-NP densities on the PHEMA-g-PEG brushes and concurrent sluggish desorption of NPs by thermal stimulus. Adsorption and desorption phenomena are further modulated by NP size yielding a system where adsorption and desorption are controlled by a delicate balance between the competitive energetics of polymer brush chelation *versus* solvation.

KEYWORDS: nanoparticles · poly(2-hydroxyethyl methacrylate) (PHEMA) · polymer brush · poly(ethylene glycol) (PEG) · surface chemistry · reversible adsorption · thermoresponsive

Nanoparticle (NP) assemblies are at the fore of diverse applications ranging from sensors to information storage, medical diagnostics, and membranes.[1–5] Early reports demonstrated that innate NP attributes are conserved within and on-top-of polymer brushes, and that NP adsorption could be directed *via* the spatially arranged chemical affinity arising from ordered phases of a block copolymer.[6–8] Recent work extended spatial patterning of substrate-anchored polymer assemblies *via* chemical affinity to post-functionalization of brushes *via* soft lithography.[9] Other studies have shown the ability to create two- and three-dimensional NP assemblies with various NP densities, in some cases using polymer brushes and by controlling brush molecular weight (MW) and grafting density.[10–18] In a series of studies, Genzer *et al*. utilized single and orthogonal polymer brush gradients to probe the effect of MW and chain density on NP density.[17,18] The effect of polymer–NP interactions has been nicely summarized in a review by Stuart,[19] while the field of responsive brush surfaces was recently reviewed by Luzinov *et al*.[20] When combined with metallic NPs (*e.g.*, Au), such NP-brush hybrid surfaces have great promise for sensor applications based on localized surface plasmon resonance.[21–24]

The majority of prior studies have focused on controlling NP distribution by elucidating how NP binding is dictated by the polymer brush architecture. The reversibility of the binding and relationship to NP size and surface chemistry has been relatively unexplored, however, especially considering synthetic (*i.e.*, nonbiological) surfaces. Conceptually, reversible control of NP–NP distance and overall density of NPs within the brush may arise from three phenomena: (1) reversible swelling–deswelling of the brush-NP hybrid *via* a solvent vapor, (2) a first-order coil-to-globule (collapse–stretching) transition of the brush within a solvent, or (3) a thermally activated absorption–desorption of NPs from or near the surface of the brush. To retain the number of NPs and only modulate NP–NP distance, the brush–NP interactions must be more robust than the solvent–brush interactions that drive the swelling–deswelling or determine the coil-to-globule transition. In this case, solvent influx will nominally increase brush volume and thus increase the mean NP–NP

*Address correspondence to richard.vaia@wpafb.af.mil.

Received for review December 1, 2008 and accepted March 24, 2009.

Published online April 1, 2009.
10.1021/nn800822c CCC: $40.75

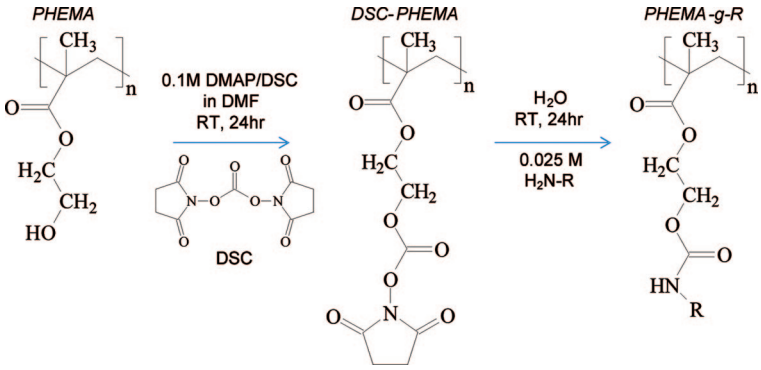

Scheme 1. Post-functionalization of poly(2-hydroxyethyl methacrylate) (PHEMA) side chain using *N,N′*-disuccinimidyl carbonate (0.1 M DSC in DMF with 0.1 M dimethylaminopyridine (DMAP)) activation and subsequent amination of the PHEMA-succinimide (DSC-PHEMA) with an amine-terminal conjugate (25 mM H_2N-R), where R is chosen from PEG_{20}, PEG_{50}, C_{16}, or C_8F_{15}.

distance. Depending on NP size, the strong binding of the NPs though is anticipated to cross-link chains and alter the underlying first-order transition with respect to a NP-free brush. Alternatively, the NP-brush interactions must be relatively weak to enable a reversible change in the surface number density of NPs through an external stimulus. Specifically, the NP number density will depend upon the number and type of interaction sites between a polymer chain and a NP. This, in turn, depends on the polymer brush density, the individual polymer chain architecture (*i.e.*, linear, branched) and NP size and surface chemistry. In the case of a coil-to-globule transition, decreased brush solubility can drive NP release. NP release may also occur by thermal activation and Brownian dynamics without the need of an underlying phase transition. The challenge in *a priori* designing reversible control of NP−NP distance or density *via* a specific phenomenon is that solvent type, brush composition and architecture, and NP size and surface chemistry may equally contribute in opposing manner to all phenomena. This implies that either process, or all, may be observable for a given system and environment.

Following this framework, this contribution discusses the use of post-polymerization functionalization of poly(2-hydroxyethyl methacrylate) PHEMA to tune the brush interactions with stable aqueous dispersion of gold nanoparticles (Au-NPs). A multidentate interaction motif enables the creation of surfaces that, depending on solvent and temperature, exhibit reversible swelling−deswelling of a stable NP−brush hybrid, as well as reversible capture and release of NPs from the brush driven by thermal activation. The reversible capture and release is affected by the MW of the grafted PEG groups. Ethylene oxide grafts with higher MW possess, on average, more chelation sites available which may interact with the Au-NPs resulting in higher average Au-NP densities and concurrently more sluggish Au-NP desorption.

RESULTS AND DISCUSSION

A general route to post-functionalization of PHEMA brushes *via* activation of the hydroxyl side chains by *N,N′*-disuccinimidyl carbonate (DSC) and subsequent coupling of primary amines (Scheme 1) has recently been reported.[9] This process allows the fabrication of a wide variety of surface functionalities without changing polymerization kinetics and enables incorporation of functionalities that are not tolerated by the polymerization process.[25] Also, the two-step nature of the activation−coupling procedure is amenable to microcontact patterning techniques, such as reactive microcontact printing. In this study, PHEMA brushes were functionalized with a variety of molecules, including amine-terminated PEG of 20 (PEG_{20}) and 50 (PEG_{50}) repeat units.[9] Details of brush functionalization are provided in the Experimental Details. In all cases, the coupling of conjugate molecules not only resulted in an increase of the thickness of the brush (as assessed by ellipsometry) but caused changes in the surface composition (as determined by X-ray photoelectron spectroscopy, XPS), and static contact angle with H_2O (Table 1).

Figure 1 depicts the relative size of the brush, chain−chain spacing, and the postfunctional oligomers based on analysis of the dry brush thickness and surface composition (see Supporting Information). XPS indicates that activation of the near-surface hydroxyl side chains of PHEMA by *N,N′*-disuccinimidyl carbonate (DSC) is almost stochiometric (Table 1). An estimate of the brush composition profile can then be derived by assuming that the extent of functionalization is high close to the tip of the brush and will decrease toward the base of the brush (close to the substrate), and that

TABLE 1. Postfunctionalization of PHEMA Brushes with Various Conjugates[a]

	thickness[b] (nm)	contact angle[c] (deg)	composition[d]	100% coupling composition[e]	coupling efficiency[f] (%)
PHEMA	14.8 ± 0.1	58 ± 2	68% C, 32% O	67% C, 33% O	N/A
DSC-PHEMA	17.2 ± 0.2	65 ± 2	62% C, 35% O, 3% N	58% C, 37% O, 5% N	~90[g]
PHEMA-g-PEG_{20}	23.8 ± 0.3	43 ± 1	67% C, 31% O, 2% N	66% C, 32% O, 2% N	79 ± 5
PHEMA-g-PEG_{50}	20.8 ± 0.3	38 ± 1	65% C, 34% O, 1% N	66% C, 33% O, 1% N	43 ± 6
PEG control[h] no activation	14.6 ± 0.3	60 ± 1	66% C, 34% O	67% C, 33% O	

[a]All reactions in table performed on the same PHEMA brush substrate. [b]Thickness measured by ellipsometry. [c]Water contact angle. [d]Elemental composition measured by XPS. [e]Expected elemental composition at 100% coupling efficiency. [f]As estimated from XPS data by carbon 1s peak deconvolution. [g]Estimated maximum activation efficiency based on coupling data. [h]Unactivated brush was exposed to reactant solution for 24 h.

the dry thickness of the brush provides an overall measure of the total volume addition of functional units. From our data, we estimate that approximately 18% of PHEMA monomers are activated by the DSC with the vast majority residing near the tip of the brush. As discussed in the Experimental Details, brush density is ~0.4 chains/nm^2 with M ≈ 18000 g/mol (N ≈ 130−140 monomers). Thus, approximately 20−25 of the monomers near the chain terminus are activated by the DSC. The increase of the dry brush volume indicates that on average 12−13 PEG_{20} and 2−3 PEG_{50} moieties are covalently coupled in the subsequent step, resulting in a tethered brush that exhibits an effective composition profile reminiscent of a block-copolymer. Therefore, swellability is expected to reflect this composition profile; for example the difference in aqueous solubility of PEG and PHEMA implies that the terminal PEG-rich portion of the brush will swell to a greater extent than the internal PHEMA dominated portion of the brush. Note though that the statistical nature of the postpolymerization functionalization approach implies the distribution of the chain architecture and composition is greater than derived from living polymerization approaches. Nevertheless, the branched architecture of the terminal end of the PEG−PHEMA conjugates residing on top of a linear brush backbone contrasts prior experimental[25] and theoretical[26] studies of linear and block-copolymer brushes, potentially affording opportunities for novel functionality (*i.e.*, faster and enhanced reversibility due to variation of the solvent quality).

Au-NP adsorption from water onto these PEG−PHEMA conjugated brushes were evaluated using either citrate-capped Au-NPs (30−100 nm, Ted Pella) or mercaptopropanesulfonate (MPS) functionalized Au-NPs made *via* a ligand exchange with aforementioned citrate-capped Au-NPs.[27] Figure 1 also summarizes the relative size difference between these Au NPs and the structural characteristics of the dry brush. Note that after substrate incubation in the Au-NP solution, thorough rinsing is necessary to remove weakly physisorbed NPs so as to leave only those NPs bound by specific brush−NP interactions (Experimental Details). For all results presented, the final density of absorbed NPs did not increase with further incubation time or increase of the concentration of NPs within the incubation solution, indicating that the values measured and discussed reflect quasi-static equilibrium (Experimental Details).

Using the PHEMA-g-PEG surfaces, the impact of NP surface chemistry, NP size, and MW of the PEG graft on the surface density of bound NPs is considered. With these insights into the characteristics determining the strength of NP−brush interactions, surfaces that retain NP coverage but exhibit reversible swelling, as well as those that reversibly capture and release NPs, are demonstrated.

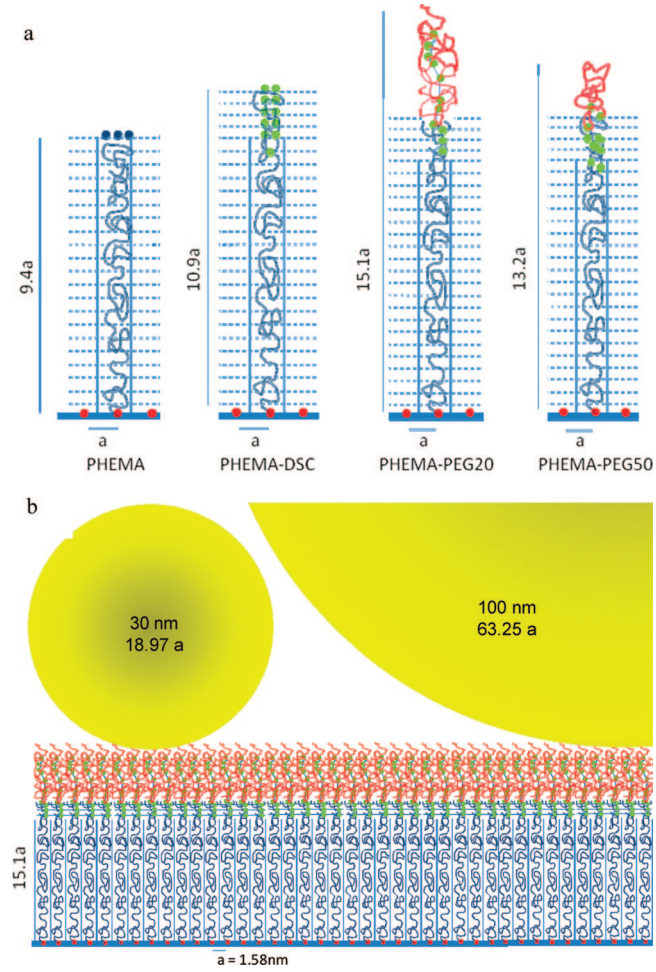

Figure 1. (a) Depiction of the relative size of the brush and spacing between chains based on analysis of the dry brush thickness and surface composition. Chain density is ~0.4 chains/nm^2 (mean chain spacing, a = 1.58 nm) with M ≈ 18000 g/mol (N ≈ 130−140 monomers). On average there are six and four monomers per chain at the surface of the dry PHEMA (blue dots) and PHEMA-DSC brush (green dots), respectively. Approximately 20−25 of the monomers near the chain terminus is activated by the DSC. The increase of the dry brush volume indicates that on average 12−13 PEG_{20} and 2−3 PEG_{50} are covalently coupled to the brush. (b) Depiction of the relative size of the PHEMA-PEG_{20} dry brush and Au NPs considered (30−100 nm). All distances are scaled by the average chain spacing, a.

PHEMA-g-PEG Interactions with Au-NPs. Prior studies demonstrated that adsorption of citrate-capped Au-NPs depended on the type of functionalization on the PHEMA brush: 1*H*,1*H*-perfluorooctylamine-modified brushes repelled the citrate-capped Au-NPs, whereas PEG-ylated surfaces adsorbed particles (30 nm in diameter) up to densities of 130 NPs/μm^2.[9] Relative to PEG_{20}, PEG_{50} showed the highest Au-NP uptake, consistent with prior observations that higher MW PEG chains stabilize gold colloids more effectively in solution. In contrast, adsorption from water of MPS-capped Au-NP is substantially weaker. Figure 2 compares the surface microstructure and XPS spectra (centering on the Au 4f region) from PHEMA-g-PEG_{50} surfaces incubated with citrate-capped and MPS-capped Au-NPs. Observations using scanning electron microscopy (SEM) show that

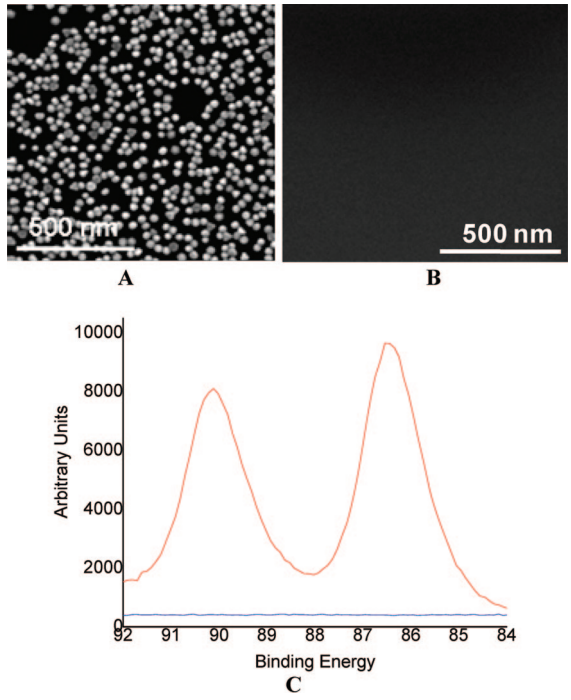

Figure 2. Scanning electron micrographs (a and b) and (c) high-resolution XPS scan (Au 4f peak) of PHEMA-g-PEG$_{50}$ surfaces incubated with 30 nm citrate-capped (a,c, red) and MPS-capped (b,c, blue) Au-NPs. Both surfaces were incubated with the respective particle solutions for 24 h and subjected to the same washing and sonication procedures (described in detail in the Experimental Details). As can be clearly seen, no Au-NPs can be detected in image b, for the brush surface exposed to the MPS-capped Au-NPs.

even the PEG-modified PHEMA brushes were completely ineffective at adsorbing MPS-capped Au-NPs. The absence of the Au 4f feature in XPS confirms the SEM observations. Similar behavior is seen for PHEMA-g-PEG$_{20}$.

This observation succinctly demonstrates that Au-NP absorption from water is not simply reflective of the relative hydrophilicity and hydrophobicity of the surface. The specific interactions between solvent, brush, and particle are all critical. Both citrate- and MPS-capped NPs are electrostatically stabilized and surrounded by hydrated cations. To the first order, the difference between these NP surfaces is that the citrate molecules are only adsorbed, whereas the MPS ligand is covalently bound to the Au-NP surface. One interpretation is that the PEG grafts displace the citrate molecules thus creating a multidentate interaction with the Au surface. Furthermore, the gain in translational freedom of the displaced citrate molecules increases the entropic contribution to the change of the chemical potential of adsorption. This is consistent with prior studies that attribute the ability of PEG to stabilize gold colloids due to the strong bonding between gold surface atoms and the pseudocrown ether structures formed by PEG.[28−33] In contrast, the MPS cannot be displaced and thus interactions take place *via* chelation of equivalent cations in the surrounding hydration sphere. Initial studies to be reported later are consistent with the MPS−PEG interactions being sensitive to pH and electrolyte content.

Since surface adsorption involves a competition between solution stability and surface binding strength per particle, the NP particle size as well as characteristics of the brush that determine possible penetrability of the NP into the brush (*e.g.*, MW and graft density) will influence the number of NPs on a surface.[34] To this end, Figure 3 summarizes the relative amount of Au (XPS Au 4f) on a PHEMA-g-PEG$_{50}$ surface after incubation with solutions of citrate-capped Au-NPs with diameters ranging from 5 to 200 nm. SEM observations of total number density and fraction of surface areas covered provide similar trends to the XPS.

In general, smaller NPs are preferentially adsorbed relative to larger particles from solutions containing the same volume fraction of Au. For instance, on the PEG$_{50}$ surfaces, a surface coverage of ~33% was measured with 10 nm particles, while surface coverage of 200 nm particles was less than 2%. Similar behavior was observed for PEG$_{20}$ substrates, but with overall lower affinity as previously mentioned (10 nm: PEG$_{20}$ surface ≈ 22% coverage; PEG$_{50}$ surface ≈ 33% coverage). On the basis of the empirical relation between molecular weight and radius of gyration, R_g, developed by Kawaguchi,[35] R_g is approximately 0.97 and 1.64 nm for PEG$_{20}$ and PEG$_{50}$, respectively. In both cases, cooperativity between adjacent PEG grafts is necessary to cover even a fraction of the surface area of a small NP (surface area, $\Sigma_{10nm} = 523$ nm^2). Given a finite penetrability of the NP into the brush, the relative contact area per NP with the surface decreases with increasing the NP diameter. This behavior is consistent with observations previously seen regarding NP size and brush penetration by Bhat *et al.*,[17,18] where it was shown that smaller particles could penetrate into the brush underlayer while large particles remained on the outer surface of the brush. This leads to an effective higher density of small particles on the polymer brush as they can access both the brush interior and surface, while large particles can only interact with chelating groups on the outer surface of the brush.

As for the impact of PEG MW, the reduced Au-NP surface coverage for the lower MW PEG$_{20}$-grafted brushes is a reflection of the brush structure. Owing to steric limitations of the postfunctionalization process, the PEG content is greater for PEG$_{20}$- than PEG$_{50}$-modified brushes, as indicated by the change in brush thickness (Δt) after grafting (PEG$_{20}$: $\Delta t \approx 9$ nm; PEG$_{50}$: $\Delta t \approx 6$ nm, Table 1). Thus if PEG content was the only factor, PHEMA-g-PEG$_{20}$ brushes should exhibit higher Au-NP density. Alternatively, the lower grafting density of PEG$_{50}$ is consistent with greater surface flexibility and potential for extended chelation afforded by a less dense arrangement of longer grafts. This would then increase the binding between a Au-NP and the brush.

To extend the single NP absorption observations, competitive absorption from aqueous solutions containing ternary NP mixtures of citrate-capped Au-NPs of varying size (30−50−80 nm and 30−50−100 nm) are summarized in Figure 4 for PHEMA-g-PEG_{50} and PHEMA-g-PEG_{20} surfaces. Here the Au-NP mixtures were created in proportions that gave equal surface area (ESA) or equal particle number density (EPN) among the NPs of different sizes. For ESA, the relative number density, n, between NPs i and j with radii r_i and r_j, respectively, is $n_j/n_i = (r_i/r_j)^2$. ESA implies that each constituent has a similar total interfacial area capable of interacting with the brush, but a different number density in solution. In contrast, equating the total EPN implies there is a greater total surface area, Σ, for the smaller particles, where $\Sigma_i/\Sigma_j = (r_i/r_j)^2$.

Consistent with the aforementioned observations, smaller NPs exhibited strong preferential absorption for a given surface functionality (PHEMA-g-PEG_{20} or PHEMA-g-PEG_{50}), irrespective of the ternary mixture composition (ESA *vs* EPN). Also, the absolute number of larger particles was greater for the ternary mixture based on EPN density. This indicates that the absorption process for NPs of this size range (30−100 nm) is determined by diffusively driven encounters between the NPs and the surface. The probability of NP absorption depends on the accessibility of the brush binding sites (greater for smaller particles), which, in turn, governs the number of collisions between NPs and the surface. This trend indicates that the binding energy per particle between PHEMA-g-PEG and citrate-capped Au-NPs is substantially greater than kT at room temperature. When comparing the length of the PEG graft, the role of surface area per NP on relative extent of absorption becomes apparent as noted above. For example, the PHEMA-g-PEG_{50} substrate had almost twice the percentage of the 80 nm particles relative to the PHEMA-g-PEG_{20} substrate (Figure 4a). A similar trend can be noted in the 30−50−100 nm ternary particle mixture (Figure 4b).

In brief, the above studies revealed that both size and surface chemistry of the Au-NPs play a crucial role in determining their uptake characteristics to PEG-functionalized PHEMA brushes. Smaller particles are adsorbed preferentially when presented at equal volume fractions. Furthermore, the MW of the graft impacts the specific size affinity in that longer brushes are capable of capturing a larger number of NPs. These guidelines enable the design of brushes with sufficiently strong binding to exhibit reversible swelling in solvent vapor or with relatively weak interactions to exhibit size-dependent, thermal reversible capture and release of NPs.

Strong NP-Brush Interactions: Reversible Swelling. When polymer brushes are exposed to a good solvent they extend from an ideal Gaussian coil into a stretched confirmation. If Au-NPs are strongly attached at high density

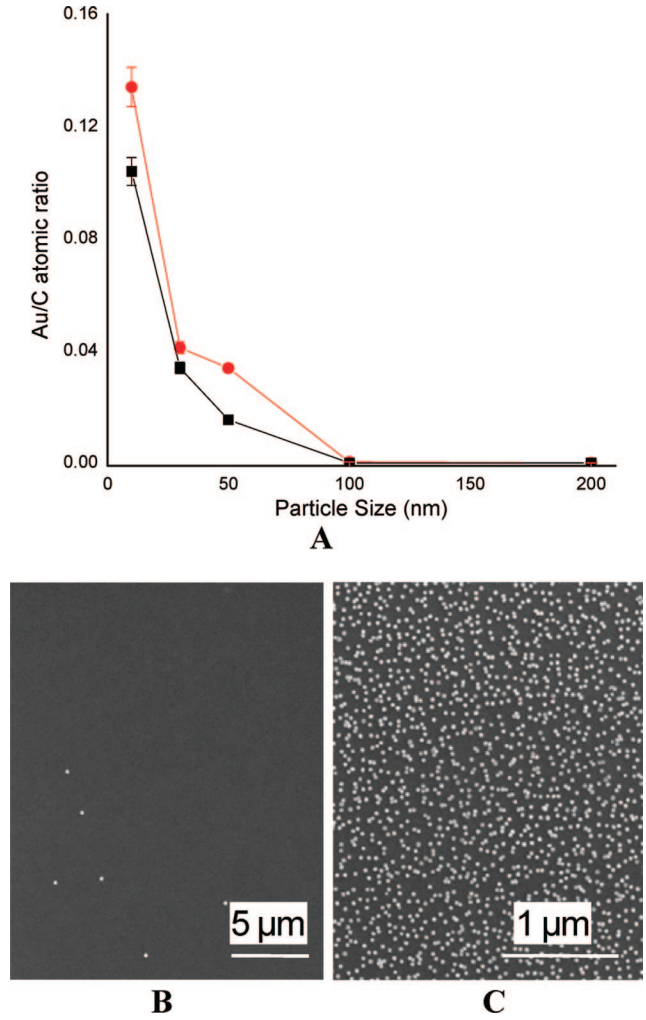

Figure 3. (a) The ratio of the Au-to-C total peak counts from XPS demonstrating a decrease in citrate-capped Au-NP absorption with increasing NP size for PEG_{20} (black line, squares) and PEG_{50} (red line, circles) grafted PHEMA brushes. All surfaces were incubated with the respective particle solutions for 24 h and subjected to the same washing and sonication procedures (described in detailed in the Experimental Details). (b and c) Representative scanning electron micrographs confirming the decreased Au-NP absorption with increasing NP size for PHEMA-g-PEG_{50} (b, 100 nm 2% coverage; c, 30 nm, 14% coverage).

to those brushes, the increase of the interparticle distances will disrupt the collective surface plasmon (localized surface plasmon resonance, LSPR) of the Au-NPs and substantially alter absorbance properties of the film. If on the other hand, the particles do not respond with the brush, and only the refractive index of the surrounding media is altered, the absorbance properties arising from the surface plasmon will merely shift a few nanometers.[36] Figure 5a shows the color of a PHEMA-g-PEG_{50} brush (on glass) with a high surface coverage (130 μm^{-2})[37] of 30 nm citrate-capped Au-NPs (e.g., Figure 3d). In the dry state, the particles are aggregated and interacting with each other thus creating a low energy, collective surface plasmon. The transmitted light gives a purplish color to the film due to the red-shifted absorbance. When the brush is swollen, such as by a

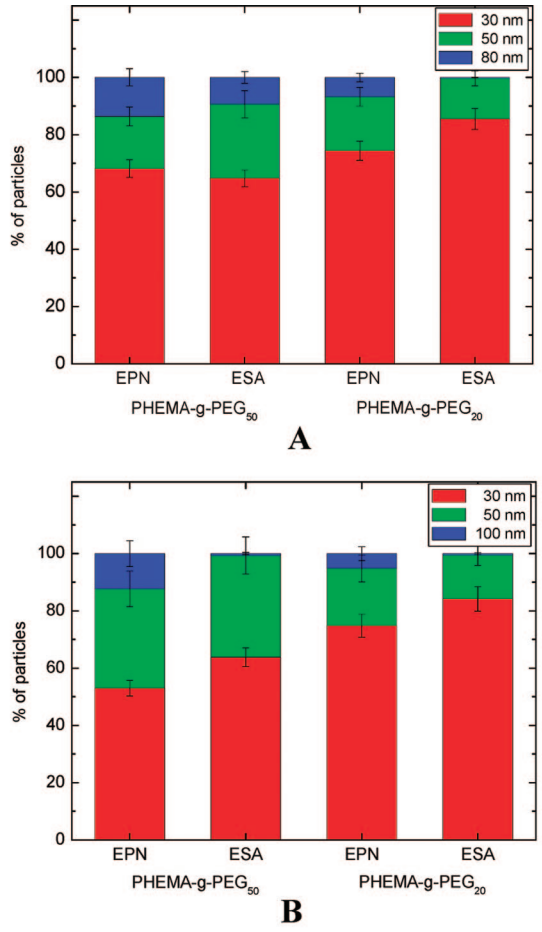

Figure 4. Percentage of adsorbed particles of different sizes from a ternary mixture of citrate-capped Au-NPs with diameters of (a) 30 (red), 50 (green), and 80 (blue) nm; and (b) 30 (red), 50 (green), and 100 (blue) nm, on PHEMA-g-PEG$_{50}$ and PHEMA-g-PEG$_{20}$ substrates. Note: EPN = equal particle number, ESA = equal surface area. (c) Representative micrograph of a ternary mixture (30−50−100 ESA) on a PHEMA-g-PEG$_{50}$ substrate.

water drop, the interparticle distance is increased, and the plasmon coupling between Au-NPs is weakened, which leads to a blue-shift in the adsorption.[38] For example a 1 μL drop of methanol will change the transmitted color from purple to pink (Figure 5b). As the methanol evaporates (15 s), the transmitted color shifts back to purple (movie: Supporting Information). This process is repeatable over at least tens of cycles without degradation of the color intensity or rate of color change. Tentative exploratory studies show that the extent of the color change and the process reversibility depend on the stability of the Au-NP−brush hybrid, and the solvent quality with respect to PHEMA and PHEMA-g-PEG. Polar solvents, such as methanol, give excellent response whereas alkanes do not alter the film color. This behavior is easy to reconcile because methanol is a good solvent for both the NPs and PHEMA-g-PEG while the swelling of PHEMA-g-PEG brushes with alkanes is problematic.

Weak NP-Brush Interactions: Thermo-reversible Capture and Release. As mentioned above, smaller NPs preferentially absorb to the PEG-grafted PHEMA brushes. Furthermore, brushes with lower MW grafted PEG chains exhibit lower densities of Au-NPs on the surfaces. Beyond affecting adsorption characteristics, these factors will also play a role in the strength of the particle-brush interaction as evidenced in desorption phenomena. Figure 6 summarizes the change in density of 30 nm citrate-capped Au-NPs on PHEMA-g-PEG$_{20}$ substrates after a thermal anneal at 85 °C in water. Substantial desorption was seen to occur after 10 min of heating, and complete desorption was seen in all cases after 60 min. When the surfaces were reincubated with a fresh solution of Au-NPs, readsorption was nearly 100% effective. This process was highly reversible over many cycles with little or no degradation of the brushes. In contrast, complete desorption of the 30 nm Au-NPs from PHEMA-PEG$_{50}$ surfaces was not achieved even after several hours of heating at 85 °C. Recall these surfaces showed a higher density of absorbed Au-NPs.

These results further suggest that the interaction strength of the Au-NPs with the PHEMA-g-PEG$_{50}$ substrates is much stronger than that of comparable size Au-NPs with the PHEMA-g-PEG$_{20}$ substrates. Either reduced penetrability associated with a higher graft density or shorter multidentate chelation per graft reduces the effective binding strength per particle such that thermal energy is sufficient to favor desorption at 85 °C. The PHEMA-g-PEG$_{50}$ surfaces required heating to the point of decomposition in order to release their strongly bound Au-NPs. The lower critical solution temperature (LCST) behavior of the PHEMA-g-PEG brush may also be argued to contribute to this behavior. PHEMA is a thermoresponsive polymer showing a cloud point at *ca.* 20−40 °C.[39] Coupling of PEG to the side chains of PHEMA increases the hydrophilicity of the brush and is likely to raise the local LCST. However as seen for poly(*N*-isopropyl acrylamide) (PNIPAM), surface confinement, chain length, and grafting alter the LCST in complex ways.[40−43] Since the observed NP release from PHEMA-g-PEG surfaces was not rapid, we do not believe an underlying first-order transition of the brush, such as a LCST, is dominating the aforementioned behavior.

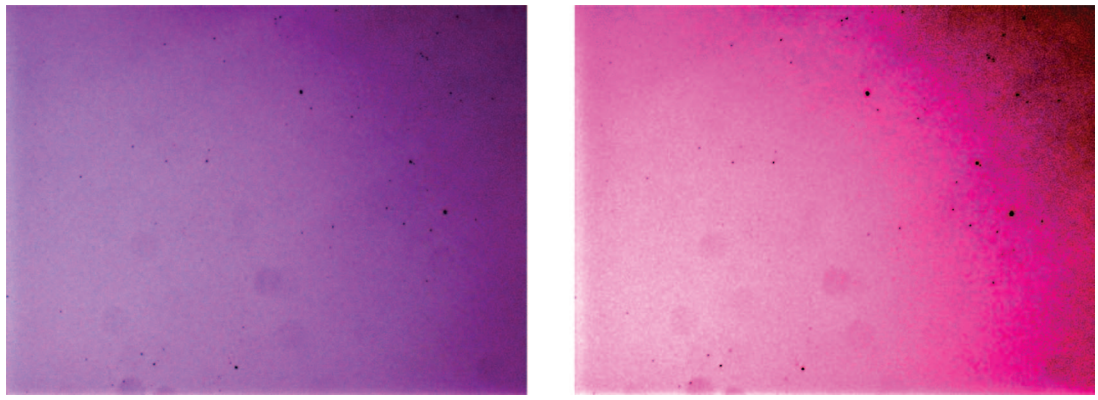

Figure 5. Optical response of Au NP−PHEMA-g-PEG_{50} hybrid in response to methanol swelling and evaporation. Change in transmitted color arises from disruption of the local surface plasmon resonance of aggregated Au NPs in the dry hybrid (left) as solvent increases the hybrid volume (right) (see movie in Supporting Information).

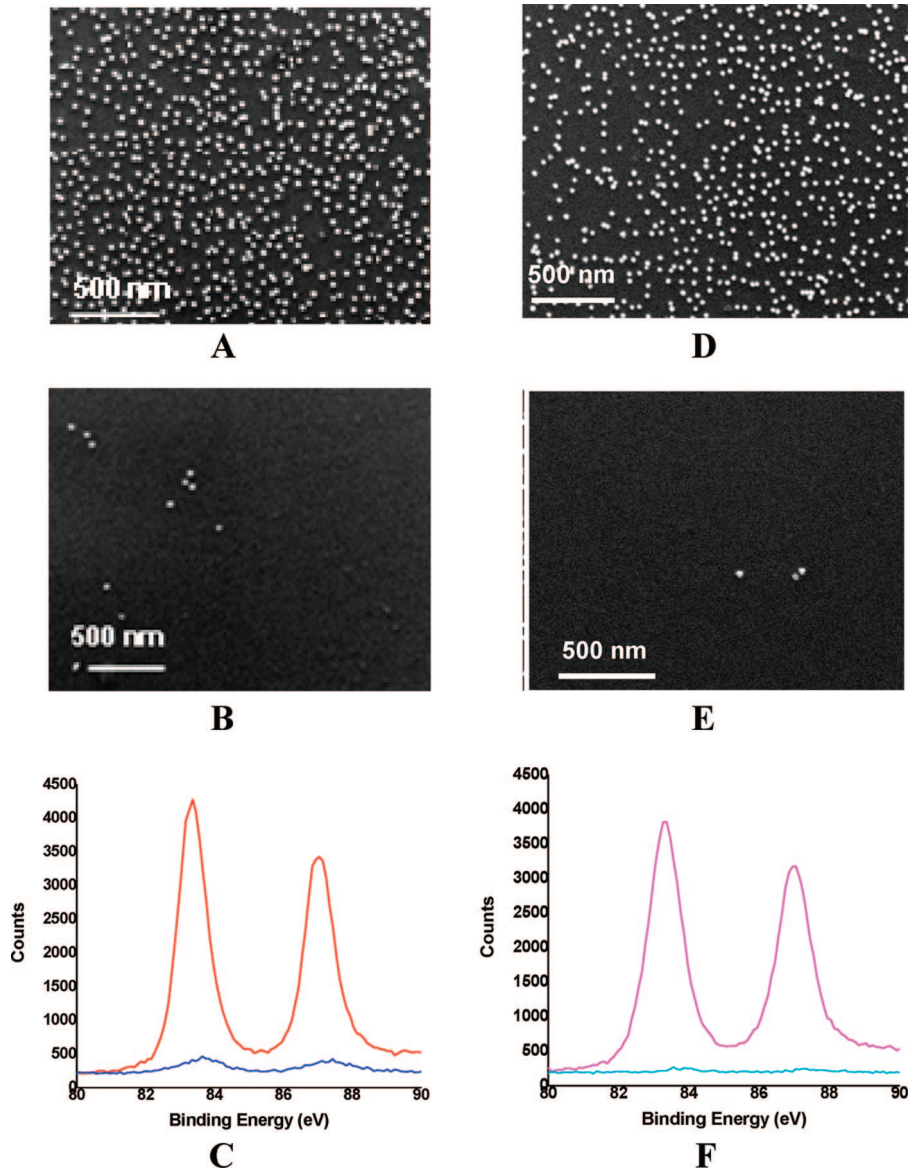

Figure 6. Scanning electron micrographs and corresponding high resolution XPS of 30 nm citrate Au-NP absorption on PHEMA-g-PEG_{20} surfaces through two absorption−desorption cycles (adsorption at room temperature, desorption at 85 °C): (a) 1st adsorption 35 ± 12 NP/μm^2; (b) 1st desorption 3 ± 1 NP/μm^2; (c) XPS (Au 4f) of 1st adsorption and desorption; (d) 2nd adsorption 34 ± 15 NP/μm^2; (e) 2nd desorption 1 ± 1 NP/μm^2; (f) XPS (Au 4f) of 2nd adsorption and desorption;

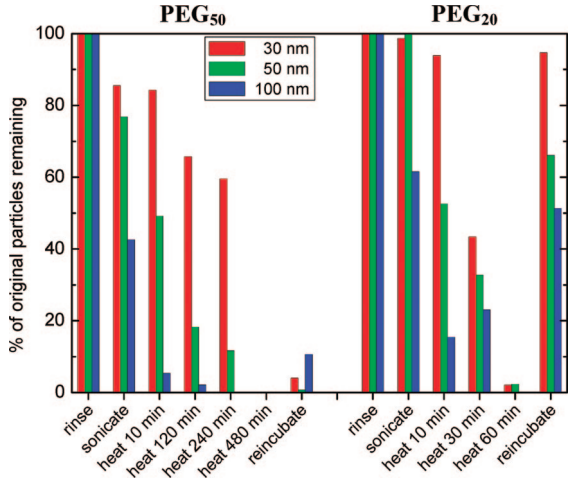

Figure 7. Desorption of 30−50−100 nm particles from PHEMA-g-PEG$_{20}$ and PHEMA-g-PEG$_{50}$ functionalized substrates.

Given that desorption qualitatively reflects absorption affinity, size-selectivity seen in Au-NP adsorption would be mirrored in desorption behavior. Following the mixed size absorption studies discussed above, Figure 7 summarizes the decrease in Au-NP density after successively more stringent desorption treatments for a ternary mixture of 30−50−100 nm particles on PHEMA-g-PEG$_{20}$ and PHEMA-g-PEG$_{50}$ surfaces. Similar trends are observed for 30−50−80 nm ternary mixtures. Note that in this experiment, the temperature was held constant at 85 °C while the heating time was varied. This contrasts with other desorption studies where surfaces are exposed to a steadily increasing temperature profile. Constant temperature desorption implies that rather than the particular temperature at any one time the total energy input into the system point is being varied. This process is widely utilized by the drug delivery community, as changes of in vivo temperature are limited, and release kinetics at physiological temperature is of utmost importance for pharmacokinetic properties.[44,45]

In general, the largest NPs desorbed with the least total added energy, followed by medium sized particles, and finally the small particles, which were extremely difficult to fully desorb, particularly from the PHEMA-g-PEG$_{50}$ substrates. To desorb a substantial percentage of the 30 nm particles, the PHEMA-g-PEG$_{50}$ substrates had to be heated for long time periods (up to 6−8 h) incurring substrate damage, after which reincubation with a fresh NP mixture was unsuccessful. Similar behavior was also noted on the adsorption and desorption of pure solutions of 30 nm particles. In contrast, the PHEMA-g-PEG$_{20}$ substrates showed a high degree of particle desorption after 60 min of heating. When these substrates were reincubated with fresh particle mixtures, nearly full recovery of small particle adsorption was detected, but adsorption of larger particles was suppressed to lower levels relative to the original incubation. This may involve surface rearrangements of the polymer chains after heating that disrupts binding of larger particles which are thought to be very sensitive to the surface configuration.

Overall, these ternary mixtures emphasize that each NP-brush interaction is independent, and thus a common substrate can capitalize on the difference in binding strength with regard to NP size to provide size-selective absorption and desorption. The larger the particle, the smaller the percentage of the particle's surface, in which a given number of PEG side-chains attached to PHEMA brushes can interact, thus limiting the total binding strength of such particles.

CONCLUSION

Polymer brush post-functionalization enables the creation of a wide variety of polymer brush/Au-NP hybrids from a common brush precursor. Activation of PHEMA hydroxyl side chains by *N*,*N*′-disuccinimidyl carbonate (DSC), and subsequent coupling of primary amines, allows for the fabrication of a wide variety of surface functionalities without altering polymerization kinetics. This variation of the surface properties of the polymer brush enables the tailoring of analyte adsorption, *i.e.*, citrate-capped Au-NPs. By changing the MW of the PEG graft attached to PHEMA backbone, the interaction strength per NP could be tuned to yield substrates in which the brush−NP hybrid exhibits reversible swelling in good solvents, as well as substrates in which size-dependent, reversible absorption−desorption cycles of NPs could be thermally activated. Tailoring the brush, however, must specifically consider the nature of the NP surface, not simply the solubility of the NP. Although forming electrostatically stabilized aqueous colloids, MPS-coated Au-NPs do not exhibit the rich diversity of absorption phenomena with PHEMA-g-PEG as do citrate-stabilized Au-NPs.

For the citrate-stabilized Au-NPs/PHEMA-g-PEG system, the diversity of absorption phenomena arises from five factors: (1) the noncovalent interactions between citrate and Au-NPs, (2) the high affinity of PEG to Au surface, (3) the multidentate interaction motif of PEG, (4) the density of PEG grafts, and (5) the size of the NP which governs the number of adsorption sites between the brush and the NP. The first two factors account for the general absorption of Au-NPs to the PHEMA-g-PEG brush. The next two factors modulate the interaction strength per NP. Higher MW PEG grafts have, on average, more chelation sites available capable of interacting with the Au-NPs. This leads to higher average Au-NP densities and more sluggish Au-NP desorption. Finally, the size, and to a lesser extent the density of PEG grafts, determine the interaction strength per particle and thus the probability that the NP will desorb due to thermal excitation. As the surface area of interaction is diminished, the energetics of surface binding will become less favorable relative to solvation.

In summary, a single conceptual platform that enables the tuning of NP−surface interactions affords a wide range of technological opportunities. Colorimetric sensors based on modulation of the localized surface plasmon resonance can be realized by creating strong NP−brush interactions. Harnessing weak NP−surface interactions that depend on NP size provides size-selective capture and release. Such dynamic control of adsorption affinity and size-selectivity will find use in microfluidic devices, laboratory-on-the-chip, and chromatographic applications, such as efficient separation media for size-sorting, separation, and purification of monodispersed particles from a polydisperse starting solution. The extension of this approach to dynamic control of biomolecule adsorption affinity possesses larger ranging implications on the biosensing field and is currently under investigation.

EXPERIMENTAL DETAILS

Materials. Unless specified all chemicals were analytical grade from Sigma-Aldrich and were used as-received. 2-Hydroxyethylmethacrylate (HEMA) was obtained from Acros, methanol (HLPC grade) was purchased from Fisher Scientific. MeO-PEG_{50}-NH_2 and MeO-PEG_{20}-NH_2 were obtained from Polymer Source. *N*,*N*′-Disuccinimidyl carbonate was purchased from Fluka (purum grade). Citrate-capped Au-NP solutions were supplied by Ted Pella. MPS-capped Au-NP solutions were synthesized *via* ligand exchange using commercial citrate-capped Au-NP solutions using a protocol described previously.[27] To ensure similar particle number concentrations in each batch, the MPS-capped Au-NP solution was allowed to evaporate at room temperature until it possessed the same optical density as the citrate-capped Au-NP solution.

Instrumentation. Samples were sonicated using a 2 Amp Sonicor (SC-101TH), with an operating frequency of ~50 kHz. Polymer brush thicknesses were measured by a variable angle ellipsometry (Senetech SE400) using a wavelength of 632.8 nm and angles ranging from 40 to 70°. Reported average thickness and error were determined from six different measurements on the same sample. Thickness was determined using the accompanying software and fitting Ψ and Δ curves from data taken at multiple angles. The bulk refractive index of 1.512 for PHEMA was assumed. Note that for film thicknesses below 20 nm, refractive index differences in the range anticipated for the postfunctionalization ($\Delta n \approx 0.1$) resulted in an insignificant change in the calculated thickness (±10%). Elemental compositions and coupling efficiencies were determined using X-ray photoelectron spectroscopy (Surface Instruments) M-probe instrument operated at a base pressure of 3×10^{-7} Pa using an operating voltage of 10 kV by averaging results from four spots (800 μm^2) on each wafer. ESCA 2000 software was used to interpret the XPS data. Contact angles were determined by using deionized water on a FTA200 instrument (First Ten Angstroms) at ~22 °C. In a given experiment with a single water drop, 30 contact angle measurements were taken over the period of 2 min and averaged. Four separate experiments were conducted per sample and the results were averaged. All samples were analyzed on the same day at 15% relative humidity. Optical microscopy was performed on a Zeiss-Axio optical microscope. Scanning electron microscopy was performed on a FEI XL30 scanning electron microscope at 20 kV at a working distance of 5.0 mm. Particle counting from SEM micrographs was performed *via* ImageJ image processing software. Details about the counting and thresholding procedures are reported in the respective experimental sections below.

Polymer Brush Synthesis. Silicon wafers (Silicon Valley Microelectronics Ltd.) were cut into pieces of desired sizes and exposed to ultraviolet radiation/ozone (UVO) treatment (Jelight Inc., model 42) for 30 min. This treatment generates a large concentration of surface-bound hydroxyl groups required for the attachment of the polymerization initiator. Poly(2-hydroxyethyl methacrylate) (PHEMA) brushes were prepared by "grafting from" polymerization based on atom transfer radical polymerization (ATRP) on account of its ability to form polymers with low polydispersity.[44] This procedure involved the deposition of the ATRP initiator (11-(2-bromo-2-methyl) propionyloxy)-undecyl trichlorosilane, BMPUS) on the surface of a silicon wafer and subsequent polymerization initiated from the surface-bound BMPUS centers. BMPUS was attached to silicon substrate by keeping a UVO-treated wafer in the initiator solution (5 mL in 150 mL anhydrous toluene at −10 °C for about 12 h). Polymerization of HEMA was carried out using methanol/water ATRP using a mixture containing 37.45 g of HEMA, 25.5 g of methanol, 7 g of water, 2.33 g of bipyridine, 0.663 g of CuCl, and 0.05 g of $CuCl_2$. The polymerization time (ranging between 2 and 5 h) was adjusted to achieve desired brush thickness and chain density of ~0.4 chains/nm^2. These pristine polymer brushes have been thoroughly characterized as reported in prior publications.[47−49] By combining ellipsometric results of dry brush thickness with SEC measurements from brushes grown on and cleaved off small particles a good estimate of grafting density and a correlation between dry brush thickness and molecular weight can be derived. From these studies it has been deduced that for brushes synthesized under the aforementioned conditions $M = 1200h$, where M is the number average molecular weight of the brush and h is the height of the dry brush in nm. Thus the brushes used in this study would have an $M \approx 18000$ g/mol.

Polymer Brush Functionalization. To ensure that the measured results were not impacted by variations of chain density or chain length on different wafers, experiments were performed on a single brush wafer that was fractured into multiple pieces. The substrates coated with PHEMA brushes were immersed in a deoxygenated solution of 0.1 M *N*,*N*′-disuccinimidyl carbonate and 4-dimethylaminopyridine in anhydrous DMF for 24 h.[9] The specimens were then rinsed thoroughly with DMF and methylene chloride and subsequently immersed in a 25 mM solution of the primary amine-containing coupling agent and kept for 24 h. After coupling, the samples were removed from the solution and sonicated for 15 min each in Milli-Q water, acetone, and methylene chloride in order to remove excess adsorbed reactants. Postfunctionalized brushes were analyzed by ellipsometry, contact angle, and XPS.

Successful coupling of PEG conjugates was demonstrated by an increase in polymer brush thickness and a concurrent decrease in the static contact angle (cf. Table 1). XPS was employed to elucidate elemental composition and chemical bonding information about the polymer brush conjugates thus providing a quantitative measure of the coupling efficiency[9] (Table 1). Control experiments, in which polymer brush surfaces were directly exposed to reactants without DSC activation, showed no substantial changes in thickness, contact angle, or elemental composition relative to the activated substrates (cf. Table 1).

Incubation of PHEMA-g-PEG Substrates in Monodispersed Nanoparticle Solutions. The postfunctionalized polymer brushes were floated on top of 200 μL solutions of either citrate-capped Au-NPs or MPS-functionalized Au-NPs (particle concentration 2.0×10^{11} particles/mL) for 24 h. This deposition arrangement (floating of brushes on solutions) was chosen so that only diffusive encounters between the NPs and the surface occurred; and any possibility of NP settling or gravity-assisted concentration gradients could be avoided. An incubation time of 24 h was chosen based on initial experiments which followed the concentration of gold nanoparticles on the surface related to the incubation time. PHEMA-g-PEG brushes were incubated for 1 h, 24 h, and 1 week in Au-NP solutions. While the samples incubated for 1 h had the lowest concentration of NPs, the concentration of NPs on the 24 h and 1 week incubated samples were within experimen-

tal error. This suggests that the adsorption/desorption/diffusion phenomena of NP interactions with the polymer brush have reached equilibrium after 24 h. After incubation, the wafers were taken out of the Au-NP solution, and rinsed thoroughly with copious amounts of Milli-Q water by dousing the wafers with a gentle stream of Milli-Q water for 2 min. The wafer was then placed in a jar of ~10 mL Milli-Q water and sonicated for 5 min. The wafer was then rinsed thoroughly with copious amounts of methanol by dousing with a gentle stream of methanol for 15 s. The wafer was then placed in a jar with ~10 mL methanol and sonicated for 5 min. At the conclusion of this sonication step, the wafer was rinsed again with methanol and gently blown dry with a stream of dry nitrogen. With the smaller sized nanoparticles (≤30 nm), the density of nanoparticles, in only rinsed and rinsed/sonicated samples was nearly identical. However, heterogeneous dense patches of nanoparticles were rarely, but sometimes, seen in the rinsed-only samples, while the rinsed/sonicated samples gave more reproducible surfaces with a more homogeneous distribution of nanoparticles.

SEM micrographs were taken from five different representative areas (area 5 μm^2) on each sample and analyzed *via* ImageJ image processing software to count the number of deposited Au-NPs and to compare the relative numbers of strongly adsorbed Au-NPs for different substrates. The averaged results and error among different sample areas are reported in the text. XPS was used to compare the total amount of gold between substrates incubated with different ligand-capped NP solutions by comparing the relative intensities of the Au 4f peaks.

Incubation of PEG-g-PHEMA Substrates in Ternary Mixtures of Different Size Nanoparticle Solutions. The brushes were floated on top of 200 μL solutions of ternary mixtures of three sizes of monodispersed citrate-capped Au-NP solutions from Ted Pella for 24 h. Ternary mixtures of comprising particles with diameters (set 1) 30, 50, and 80 nm and (set 2) 30, 50, and 100 nm citrate-capped Au-NPs were obtained by mixing the proper proportion of the different monodispersed Au-NP solutions. Two series of Au-NP solutions were prepared: (a) each particle size set had the same surface area in the mixture, (b) the particle number concentration of each particle size was the same in the mixture. To establish the proper amount of Au-NPs, we used nominal particle size and solution particle concentrations provided by Ted Pella. For example, to obtain 200 μL of a ternary particle solution with equivalent particle concentrations for 30, 50, and 80 nm particles, with solution concentrations of 2.0×10^{11} particles/mL, 4.5×10^{10} particles/mL, and 1.1×10^{10} particles/mL, respectively, one mixes 8.5 μL of 30 nm NP solution, 37 μL of 50 nm NP solution, and 154 μL of 80 nm NP solution to give an ~200 μL solution with an overall concentration of 2.2×10^9 particles/mL of each particle. To generate solutions with equal surface area per particle the appropriate amounts of NP solutions are normalized using surface area of each particle size (assuming that all particles are monodisperse in size and have a shape of a perfect sphere). After incubation, the substrates containing Au-NPs attached to the functionalized brushes were taken out of the Au-NP solution and rinsed only (no sonication) with Milli-Q water and methanol in order to desorb any weakly bound Au-NPs. This rinsing process is described in detail in the section "Incubation of PHEMA-g-PEG Substrates in Monodispersed Nanoparticle Solutions". SEM micrographs were taken from five different representative areas (area 5 μm^2) on each sample and analyzed *via* ImageJ image processing software to count the number of deposited Au-NPs and to compare the relative numbers of strongly adsorbed Au-NPs for different size NPs. Particles were binned into their respective size categories from the dispersed mix of different size particles by allowing only particles with size ±10% from the reported value to be counted in that grouping, all other particles were excluded. For example, for the 30 nm particle bin all particles reported by ImageJ of having sizes 27.0−33.0 nm were included, particles of 45.0−55.0 nm were included in the 50 nm bin, and particles of 72−88 nm were included in the 80 nm bin.

Thermoreversible Capture and Release of Citrate-Capped Gold Nanoparticles. The postfunctionalized polymer brushes were floated on top of 200 μL solutions of 30 nm citrate-capped Au-NPs from Ted Pella (particle concentration 2.0×10^{11} particles/mL) for 24 h. After incubation, the wafers were taken out of the Au-NP solution and rinsed and sonicated for 5 min each in Milli-Q water and methanol in order to desorb weakly bound Au-NPs. The substrates were then characterized by SEM and XPS as follows. SEM micrographs were taken from five different representative areas (area 5 μm^2) on each sample and analyzed *via* ImageJ image processing software to count the number of deposited Au-NPs and to compare the relative numbers of strongly adsorbed Au-NPs for different substrates. XPS was employed to compare the total amount of gold between adsorption and desorption cycles by comparing the relative intensities of the Au 4f peaks for the different cycles. After analysis the substrates were placed in a bath of Milli-Q water, thermostatted at 85 °C for 60 min. After this time the wafers were removed and washed and sonicated as before and analyzed by XPS and SEM as previously described. After analysis the wafers were floated on top of a fresh solution of 30 nm citrate-capped Au-NP solutions from Ted Pella for 24 h as previously described. Surface characterization using SEM and XPS, as described above, followed. Finally, the desorption process was repeated. As a control, a MeO-PEG_{20}-NH_2-functionalized wafer piece was exposed to 30 nm citrate-capped Au-NP solutions from Ted Pella for 24 h as described above. However, instead of placing the specimen in a hot water bath, it was left in Milli-Q water at room temperature for 24 h. No significant desorption was noted by XPS or SEM analysis.

To examine the size selectivity of desorption, ternary mixtures of 30−50−80 nm and 30−50−100 nm Au-NPs were prepared as described above. The size-selective release properties of these equal surface area density particle mixtures were then examined by using increasingly stringent desorption conditions. The wafers were sonicated for 5 min each in methanol and Milli-Q water and analyzed as previously described. After initial analysis the substrates were placed in a bath of Milli-Q water, thermostatted at 85 °C for increasing amounts of time. After each exposure to the hot water bath the wafers were characterized by SEM as previously described. This procedure was repeated until most of the particles were desorbed from the brush substrate. The substrates were then reincubated with fresh mixtures of NPs as previously described and reanalyzed by SEM.

Acknowledgment. The authors would like to acknowledge Sarah Lane for her helpful contributions to the schematics in this publication, John Grant and Benjamin Philips for their expert assistance with X-ray photoelectron spectroscopy and helpful discussions, and Robert MacCuspie for assistance with Image J processing software and helpful discussions. The authors would also like to acknowledge the Office of Naval Research (Grant No. N-00014-5-01-0613) for financial assistance.

Supporting Information Available: Calculations for changes in dry brush thickness; movie showing swell−deswell cycle of Au-NP PHEMA-PEG. This material is available free of charge *via* the Internet at http://pubs.acs.org.

REFERENCES AND NOTES

1. Maie-Christine Daniel, M-C.; Astruc, D. Gold Nanoparticles: Assembly, Supramolecular Chemistry, Quantum-Size-Related Properties, and Applications toward Biology, Catalysis, and Nanotechnology. *Chem. Rev.* **2004**, *104*, 293–346.
2. Bhat, R. R.; Genzer, J. Combinatorial Study of Nanoparticle Dispersion in Surface-Grafted Macromolecular Gradients. *Appl. Surf. Sci.* **2006**, *252*, 2549–2554.
3. Fendler, J. H. *Nanoparticles and Nanostructured Films: Preparation, Characterization, and Applications;* Wiley-VCH: New York, 1998.
4. Alivisatos, A. P. Semiconductor Clusters, Nanocrystals, and Quantum Dots. *Science* **1996**, *271*, 933–937.
5. Weller, H. Colloidal Semiconductor Q-Particles: Chemistry in the Transition Region Between Solid State and Molecules. *Angew. Chem., Int. Ed.* **1993**, *32*, 41–53.
6. Sohn, B. H.; Cohen, R. E. Processible Optically Transparent Block Copolymer Films Containing Superparamagnetic Iron Oxide Nanoclusters. *Chem. Mater.* **1997**, *9*, 264–269.

7. Hashimoto, T.; Harada, M.; Sakamoto, N. Incorporation of Metal Nanoparticles into Block Copolymer Nanodomains *via* in-Situ Reduction of Metal Ions in Microdomain Space. *Macromolecules* **1999**, *32*, 6867–6870.
8. Ciebien, J. F.; Clay, R. T.; Sohn, B. H.; Cohen, R. E. Brief Review of Metal Nanoclusters in Block Copolymer Films. *New J. Chem.* **1998**, *22*, 685–691.
9. Diamanti, S.; Arifuzzaman, S.; Elsen, A.; Genzer, J.; Vaia, R. Reactive Patterning *via* Post-Functionalization of Polymer Brushes Utilizing Disuccinimidyl Carbonate Activation to Couple Primary Amines. *Polymer* **2008**, *49*, 3770–3779.
10. Currie, E. P. K.; van der Gucht, J.; Borisov, O. V.; Cohen Stuart, M. A. End-Grafted Polymers with Surfactants: A Theoretical Model. *Langmuir* **1998**, *14*, 5740–5750.
11. Currie, E. P. K.; Fleer, G. J.; Cohen Stuart, M. A.; Borisov, O. V. Grafted Polymers with Annealed Excluded Volume: A Model for Surfactant Association in Brushes. *Eur. Phys. J. E* **2000**, *1*, 27–40.
12. Gage, R. A.; Currie, E. P. K.; Cohen Stuart, M. A. Adsorption of Nanocolloidal SiO_2 Particles on PEO Brushes. *Macromolecules* **2001**, *34*, 5078–5080.
13. Liu, Z.; Pappacena, K.; Cerise, J.; Kim, J.; Durning, C. J.; O'Shaughnessy, B.; Levicky, R. Organization of Nanoparticles on Soft Polymer Surfaces. *Nano Lett.* **2002**, *2*, 219–224.
14. Collier, C. P.; Vossmeyer, T.; Heath, J. R. Nanocrystal Superlattices. *Annu. Rev. Phys. Chem.* **1998**, *49*, 371–404.
15. Pileni, M. P. Self-Assemblies of Nanocrystals: Fabrication and Collective Properties. *Appl. Surf. Sci.* **2001**, *171*, 1–14.
16. Murray, C. B.; Kegan, C. R.; Bawendi, M. G. Synthesis and Characterization of Monodisperse Nanocrystals and Close-Packed Nanocrystal Assemblies. *Annu. Rev. Mater. Sci.* **2000**, *30*, 545–610.
17. Bhat, R. R.; Genzer, J.; Chaney, B. N.; Sugg, H. W.; Liebmann-Vinson, A. Controlling the Assembly of Nanoparticles Using Surface Grafted Molecular and Macromolecular Gradients. *Nanotechnology* **2003**, *14*, 1145–1152.
18. Bhat, R. R.; Tomlinson, M. R.; Genzer, J. Orthogonal Surface-Grafted Polymer Gradients: A Versatile Combinatorial Platform. *J. Polym. Sci., Part B: Polym. Phys.* **2005**, *43*, 3384–3394.
19. Currie, E. P. K.; Norde, W.; Stuart, C. M. A. Tethered Polymer Chains: Surface Chemistry and Their Impact on Colloidal and Surface Properties. *Adv. Colloid Interface Sci.* **2003**, *100−102*, 205–265.
20. Luzinov, I.; Minko, S.; Tsukruk, V. V. Responsive Brush Layers: from Tailored Gradients to Reversibly Assembled Nanoparticles. *Soft Matter* **2008**, *4*, 714–725.
21. Tokareva, I.; Minko, S.; Fendler, J. H.; Hutter, E. Nanosensors Based on Responsive Polymer Brushes and Gold Nanoparticle Enhanced Transmission Surface Plasmon Resonance Spectroscopy. *J. Am. Chem. Soc.* **2004**, *126*, 15950–15951.
22. Lupitskyy, R.; Motornov, M.; Minko, S. Single Nanoparticle Plasmonic Devices by the "Grafting to" Method. *Langmuir* **2008**, *24*, 8976–8980.
23. Tokarev, I.; Tokareva, I.; Minko, S. Gold-Nanoparticle-Enhanced Plasmonic Effects in a Responsive Polymer Gel. *Adv. Mater.* **2008**, *20*, 2730–2734.
24. Link, S.; El-Sayed, M. A. Shape and Size Dependence of Radiative, Non-Radiative and Photothermal Properties of Gold Nanocrystals. *Int. Rev. Phys. Chem.* **2000**, *19*, 409–453.
25. Advincula, R. C.; Brittain, W. J.; Caster, K. C.; Ruhe, J. *Polymer Brushes: Synthesis, Characterization, Applications*; Wiley-VCH: Germany, 2004.
26. Szleifer, I.; Carignano, M. A. Tethered polymer layers: phase transitions and reduction of protein adsorption. *Macromol. Rapid Commun.* **2000**, *21*, 423–448.
27. Voevodin, A. A.; Vaia, R. A.; Patton, S. T.; Diamanti, S. J.; Pender, M.; Yoonesi, M.; Brubaker, J.; Hu, J. H.; Sanders, J. H.; Phillips, B. S.; MacCuspie, R. I. Nanoparticle-Wetted Surfaces for Relays and Energy Transmission Contacts. *Small* **2007**, *3*, 1957–1963.
28. Longenberger, L.; Mills, G. Formation of Metal Particles in Aqueous Solutions by Reactions of Metal Complexes with Polymers. *J. Phys. Chem.* **1995**, *99*, 475–478.
29. Sakai, T.; Alexandridis, P. Size- and shape-controlled synthesis of colloidal gold through autoreduction of the auric cation by poly(ethylene oxide)−poly(propylene oxide) block copolymers in aqueous solutions at ambient conditions. *Nanotechnology* **2005**, *16*, S344−S353.
30. Sakai, T.; Alexandridis, P. Mechanism of Gold Metal Ion Reduction, Nanoparticle Growth and Size Control in Aqueous Amphiphilic Block Copolymer Solutions at Ambient Conditions. *J. Phys. Chem. B* **2005**, *109*, 7766–7777.
31. Hirai, H.; Toshima, N. *Tailored Metal Catalysts;* D. Reidel: Dordrecht, The Netherlands, 1986.
32. Hayat, M. A. *Colloidal Gold, Principles, Methods and Applications*; Academic Press: New York, 1989.
33. Hiramatsu, H.; Osterloh, F. E. A Simple Large-Scale Synthesis of Nearly Monodisperse Gold and Silver Nanoparticles with Adjustable Sizes and with Exchangeable Surfactants. *Chem. Mater.* **2004**, *16*, 2509–2511.
34. Kim, J. U.; O'Shaughnessy, B. Morphology Selection of Nanoparticle Dispersions by Polymer Media. *Phys. Rev. Lett.* **2002**, *89*, 238301-1–238301-4.
35. Kawaguchi, S.; Imai, G.; Suzuki, J.; Miyahara, A.; Kitano, T. Aqueous-Solution Properties of Oligo-(Ethylene Oxide) and Poly(Ethylene Oxide) by Static Light-Scattering and Intrinsic-Viscosity. *Polymer* **1997**, *38*, 2885−2891 ($r_g = 0.020M^{0.58}$).
36. Tokareva, I.; Minko, S.; Fendler, J. H.; Hutter, E. Nanosensors Based on Responsive Polymer Brushes and Gold Nanoparticle Enhanced Transmission Surface Plasmon Resonance Spectroscopy. *J. Am. Chem. Soc.* **2004**, *126*, 15950–15951.
37. Note: Au-NP density on glass slides could not be directly measured by scanning electron microscopy due to charging of the substrate. However, the brush samples were synthesized in an analogous manner to those on silicon substrates and are thus expected to have similar Au-NP densities.
38. Ung, T.; Liz-Marzan, L. M.; Mulvaney, P. Gold Nanoparticle Thin Films. *Colloids Surf., A* **2002**, *202*, 119–126.
39. Weaver, J. V. M.; Bannister, I.; Robinson, K. L.; Bories-Azeau, X.; Armes, S. P; Smallridge, M.; McKenna, P. Stimulus-Responsive Water-Soluble Polymers Based on 2-Hydroxyethyl Methacrylate. *Macromolecules* **2004**, *37*, 2395–2403.
40. Yim, H.; Kent, M. S.; Mendez, S.; Balamurugan, S. S.; Balamurugan, S.; Lopez, G. P.; Satija, S. Temperature-Dependent Conformational Change of PNIPAM Grafted Chains at High Surface Density in Water. *Macromolecules* **2004**, *37*, 1994–1997.
41. Yim, H.; Kent, M. S.; Satija, S.; Mendez, S.; Balamurugan, S. S.; Balamurugan, S.; Lopez, G. P. Study of the Conformational Change of Poly(*N* -Isopropylacrylamide)-Grafted Chains in Water with Neutron Reflection: Molecular Weight Dependence at High Grafting Density. *J. Polym. Sci. B* **2004**, *42*, 3302–3310.
42. Yim, H.; Kent, M. S.; Mendez, S.; Lopez, G. P.; Satija, S.; Seo, Y. Effects of Grafting Density and Molecular Weight on the Temperature-Dependent Conformational Change of Poly(*N*-isopropylacrylamide) Grafted Chains in Water. *Macromolecules* **2006**, *39*, 3420–3426.
43. Zhu, X.; Yan, C.; Winnik, F. M.; Leckband, D. End-Grafted Low-Molecular-Weight PNIPAM Does Not Collapse above the LCST. *Langmuir* **2007**, *23*, 162–169.
44. Klouda, L.; Mikos, A. G. Thermoresponsive Hydrogels in Biomedical Applications. *Eur. J. Pharm. Biopharm.* **2008**, *68*, 34–45.
45. Bhattarai, N.; Ramay, H. R.; Gunn, J.; Matsen, F. A.; Zhang, M. PEG-Grafted Chitosan as an Injectable Thermosensitive Hydrogel for Sustained Protein Release. *J. Controlled Release* **2005**, *103*, 609–624.

46. Patten, T. E.; Matyjaszewski, K. Atom Transfer Radical Polymerization and the Synthesis of Polymeric Materials. *Adv. Mater.* **1998**, *10*, 901–915.
47. Wu, T.; Efimenko, K.; Vlcek, P.; Subr, V.; Genzer, J. Formation and Properties of Anchored Polymers with a Gradual Variation of Grafting Densities on Flat Substrates. *Macromolecules* **2003**, *36*, 2448–2453.
48. Tomlinson, M. R.; Genzer, J. Evolution of Surface Morphologies in Multivariant Assemblies of Surface-Tethered Diblock Copolymers after Selective Solvent Treatment. *Langmuir* **2005**, *21*, 11552–11555.
49. Wu, T.; Efimenko, K.; Genzer, J. Combinatorial Study of the Mushroom-to-Brush Crossover in Surface Anchored Polyacrylamide. *J. Am. Chem. Soc.* **2002**, *124*, 9394–9395.